Deposition of environmentally relevant nanoplastic models in sand during transport experiments

Alice Pradel, Hind El Hadri, Cloé Desmet, Jessica Ponti, Stephanie Reynaud, Bruno Grassl, Julien Gigault

Deposition of environmentally relevant nanoplastic models in sand during transport experiments

Alice Pradel, Hind el Hadri, Cloé Desmet, Jessica Ponti, Stéphanie Reynaud, Bruno Grassl, Julien Gigault

PII: S0045-6535(20)31105-X

DOI: https://doi.org/10.1016/j.chemosphere.2020.126912

Reference: CHEM 126912

To appear in: *ECSN*

Received Date: 9 February 2020

Revised Date: 17 April 2020

Accepted Date: 26 April 2020

Please cite this article as: Pradel, A., Hadri, H.e., Desmet, Cloé., Ponti, J., Reynaud, Sté., Grassl, B., Gigault, J., Deposition of environmentally relevant nanoplastic models in sand during transport experiments, *Chemosphere* (2020), doi: https://doi.org/10.1016/j.chemosphere.2020.126912.

Deposition of Environmentally Relevant Nanoplastic Models in Sand during Transport Experiments

Alice Pradel [a*], Hind el Hadri [b], Cloé Desmet[c], Jessica Ponti[c], Stéphanie Reynaud [b], Bruno Grassl [b], Julien Gigault [a*]

[a] *Univ Rennes, CNRS, Géosciences Rennes - UMR 6118, 35000 Rennes, France*
[b] *IPREM, UMR 5254, CNRS-Université de Pau et des Pays de L'Adour, 64000 Pau, France*
[c] *European Commission, Joint Research Centre (JRC), Directorate F - Health, Consumers and Reference Materials, Via E. Fermi 2749, 21027 Ispra, VA, Italy*
**julien.gigault@univ-rennes1.fr*

CRediT authorship contribution statement

- Alice Pradel: Conceptualization, Methodology, Investigation, Formal analysis, Writing - original draft, review & editing, Visualization.
- Hind el Hadri: Preparation of nanoplastic models.
- Cloé Desmet: Characterization of Particle Hydrophobicity.
- Jessica Ponti: Transmission Electron Microscopy Analysis.
- Stéphanie Reynaud: Preparation of nanoplastic models.
- Bruno Grassl: Conceptualization, Writing - review and editing.
- Julien Gigault: Conceptualization, Formal analysis, Writing - review and editing, Funding acquisition.

Deposition of Environmentally Relevant Nanoplastic Models in Sand during Transport Experiments

Alice Pradel [a*], Hind el Hadri [b], Cloé Desmet[c], Jessica Ponti[c], Stéphanie Reynaud [b], Bruno Grassl [b], Julien Gigault [a*]

[a] *Univ Rennes, CNRS, Géosciences Rennes - UMR 6118, 35000 Rennes, France*
[b] *IPREM, UMR 5254, CNRS-Université de Pau et des Pays de L'Adour, 64000 Pau, France*
[c] *European Commission, Joint Research Centre (JRC), Directorate F - Health, Consumers and Reference Materials, Via E. Fermi 2749, 21027 Ispra, VA, Italy*
julien.gigault@univ-rennes1.fr

Abstract

Nanoplastics (NPTs) are defined as colloids that originated from the unintentional degradation of plastic debris. To understand the possible risks caused by NPTs, it is crucial to determine how they are transported and where they may finally accumulate. Unfortunately, although most sources of plastic are land-based, risk assessments concerning NPTs in the terrestrial environmental system (soils, aquifers, freshwater sediments, etc.) have been largely lacking compared to studies concerning NPTs in the marine system. Furthermore, an important limitation of environmental fate studies is that the NPT models used are questionable in terms of their environmental representativeness. This study describes the fate of different NPT models in a porous media under unfavorable (repulsive) conditions, according to their physical and chemical properties: average hydrodynamic diameters (200 to 460 nm), composition (polystyrene with additives or primary polystyrene) and shape (spherical or polymorphic). NPTs that more closely mimic environmental NPTs present an inhomogeneous shape (i.e., deviating from a sphere) and are more deposited in a sand column by an order of magnitude. This deposition was attributed in part to physical retention, as confirmed by the straining that occurred for the larger size fractions. Additionally, different Derjaguin-Landau-Verwey-Overbeek (DLVO) models -the extended DLVO (XDLVO) and a DLVO modified by surface element integration (SEI) method- suggest that the environmentally relevant NPT models may alter its orientation to diminish repulsion from the sand surface and may find enough kinetic energy to deposit in the primary energetic minimum. These results point to the importance of choosing environmentally relevant NPT models.

Keywords: Nanoplastic; Size; Shape; Transport; Soil; Column

1. Introduction:

It has been established that every environmental system contains plastic debris (Bank and Hansson, 2019). The marine environment is the first system in which plastic pollution has been extensively studied, probably due to the highly visible accumulation that started in the 1970s (Carpenter and Smith, 1972; Cozar et al., 2014; Law et al., 2010; Schwarz et al., 2019). Since then, the extent of this contamination has been more closely described. Plastic fragments or additives are found in remote areas as they can travel long distances (Jamieson et al., 2017; Peng et al., 2020). They have reached uninhabited forests after undergoing atmospheric transport (Allen et al., 2019) and have been incorporated into Artic sea ice after being transported by oceanic currents (Obbard et al., 2014). It is generally agreed upon that the terrestrial system is the major source of plastic waste (Jambeck et al., 2015). However, plastics in terrestrial and freshwater environments have received little attention (Horton et al., 2017; Rillig, 2012; Wagner et al., 2014). Plastic accumulates in the terrestrial system due to common sources, such as faulty waste management systems, spreading of sewage sludge, use of plastic mulches and other plastic products in agriculture, and tire wear particles (Carr et al., 2016; He et al., 2018; Liu et al., 2019; Scheurer and Bigalke, 2018). This rapidly accumulating plastic in soils and sediments can be degraded by photo-oxidation, thermo-oxidation, abrasion and biodegradation, which causes the inevitable release of small plastic particles (Huerta Lwanga et al., 2017; Ng et al., 2018). In the terrestrial system (soils, aquifers, sediments, etc.), studies have generally focused on microplastics (1 μm to 5 mm) (Dong et al., 2019a, 2019b; He et al., 2018; Liu et al., 2019; Tufenkji and Elimelech, 2005), although it is clear that plastic fragmentation does not stop at the micrometer size (Gigault et al., 2016; Lambert and Wagner, 2016).

The fragmentation of macro- and microplastics to nanoplastics (<1 μm) adds complexity to the global plastic waste issue. Even if no clear definition of nanoplastics (NPTs) is proposed by policy-makers, a scientific consensus has been proposed to define NPTs as colloids that originate from the unintentional degradation of plastic (Gigault et al., 2018; Hartmann et al., 2019). Compared to microplastics, NPTs acquire colloidal properties and become unaffected by gravity. At this scale, the fate of NPTs will be controlled by surface properties, shape and diffusion rather than by the bulk

properties (Hiemenz and Rajagopalan, 1997). The fact that the majority of plastic debris cannot be located by mass budgets at the ocean surface suggests that part of the missing fraction of plastic debris could be composed of fractions smaller than 300 µm in size (Albert A Koelmans et al., 2017; van Sebille et al., 2015). Since the nanoscale characteristics of plastic debris may pose potential risks, it is therefore crucial to determine where this plastic originates from and where it accumulates (Galloway, 2015; Albert A. Koelmans et al., 2017; Lehner et al., 2019).

Due to limited data on the occurrence of NPTs, lab-scale models can aid in determining the transfer of NPTs from one environmental system to another. For the terrestrial system, a saturated sand column is generally used as a proxy for the study of colloid transfer in soils, sediments and aquifers (Geitner et al., 2017; Lecoanet et al., 2004; Petosa et al., 2010; Redman et al., 2004; Syngouna and Chrysikopoulos, 2013; Tufenkji and Elimelech, 2004). Quevedo and Tufenkji compared the transport of spherical and size standardized polystyrene nanoparticles in quartz sand and loamy soil in the presence of monovalent or divalent salts (Quevedo and Tufenkji, 2012). Recently, Hu et al. used quartz sand columns to investigate the cotransport of naphthalene with polystyrene nanoparticles (Hu et al., 2020). Another recent work demonstrated the influence of the soil type on the same nanoparticles (Wu et al., 2019). While these works highlight the importance and complexity of the transport mechanisms in soils, they only focused on NPT models that are not representative of the NPTs found in our environment (Ter Halle et al., 2017). Indeed, the composition, shape, size, and surface are known to play key roles in the transport of nanoparticles in the environment (Hotze et al., 2010; Pelley and Tufenkji, 2008; Salerno et al., 2006). Such parameters have only recently been investigated, with studies concerning UV-aged NPTs (Liu et al., 2019) and polystyrene NPTs containing different surface functionalities (Dong et al., 2019b).

Before investigating the influence of the soil properties, the objective of the present work is to investigate how the properties of NPTs affect their transport or accumulation in soils. Thus, different NPT models were used. All models were composed of polystyrene, since this is the only commercially available nanometer-sized plastic particle available. On the one hand, both commercial and noncommercial polystyrene latex spheres (PSL), *PSL COOH* and *PSL COOH-P*, respectively, are

synthesized by a bottom-up process (Pessoni et al., 2019). This makes them highly spherical and monodisperse and it allows their surface to be modified by the addition of carboxylate functional groups (COOH), which are common on weathered plastics (Gewert et al., 2015). On the other hand, *NPT-P* are synthesized from a top-down method, which mimics the environmental mechanism of abrasion (Hadri et al., 2020). They have polymorphic (asymmetrical & irregular) shapes, a polydisperse size distribution, and they may contain some oxidized functional groups. The transport of *NPT-P* models through a sand column shows that their irregular shape will increase their probability of accumulating in porous media. These results stress the importance of choosing NPT models that have environmentally relevant physicochemical properties.

2. Methods

2.1 Dispersions of nanoplastic models

Table 1 presents the different NPT models used in the study. Carboxylated polystyrene latex spheres of 200 nm (*PSL COOH 200*) were Polybead® Carboxylate Orange Dyed Microspheres 0.20 µm purchased from (Polysciences© Warrington USA). These particles contain additives for stabilizing purposes, whose composition and concentration are unknown. To study the effect of particle composition, additive-free particles composed of primary (*-P*) polystyrene were also used. Soap and metal-free carboxylated polystyrene spheres of 430 nm (*PSL COOH 430-P*) were produced by emulsion polymerization according to the method described by Pessoni et al.(2019). Finally, NPT models with polymorphic (asymmetrical and irregular) shapes and with an average hydrodynamic diameter of 350 nm or 460 nm (*NPT 350-P* and *NPT 460-P*, respectively) were formulated from mechanically crushed PS pellets, according to the method previously described (Hadri et al., 2020). All suspensions were composed of NaCl at a concentration of 5.0 10^{-3} M with pH fixed at 6.5.

Table 1: Summary of the physicochemical properties of the nanoplastic models studied

Model name	z-average diameter d_{zH} (nm)	Polydispersity Index (PDI)	Area Equivalent Diameter (nm)	Aspect Ratio	Asperity Frequency (nm^{-1}) and *Amplitude (nm)*	Zeta potential (mV)	Particle Concentration ($\# L^{-1}$)
PSL COOH 200	200 ± 13	0.04 ± 0.03	193 ± 3	1.01 ± 0.01	0 *0*	-38.65 ± 2.23	$1.14\ 10^{12}$
PSL COOH 430-P	430 ± 28	0.07 ± 0.01	430 ± 19	1.01 ± 0.01	0.013 *12 ±2*	-29.07 ± 1.81	$1.14\ 10^{11}$
NPT 350-P	350 ± 10	0.11	244 ± 133	1.67 ± 0.56	0.013 *11 ±6*	-33.54 ± 2.72	$2.12\ 10^{11}$
NPT 460-P	460 ± 25	0.19	329 ± 223	1.68 ± 0.58			$9.34\ 10^{10}$

2.2 Charge characterization

The zeta potential of the particles was assessed using a Wallis zetameter by Cordouan Technologies (Pessac, France). The particles were suspended in the same mobile phase as that used for the experimental conditions: NaCl at $5.0\ 10^{-3}$ M and pH 6.5. The electrophoretic mobility of the colloidal particles was converted into a zeta potential by using Smoluchowski's formula. A zeta potential for sand of -50 mV was chosen according to Vinogradov et al. (2010).

2.3 Size characterization

Hydrodynamic diameters (d_H) were determined by dynamic light scattering (DLS) using a Vasco-Flex particle size analyzer (Cordouan Technologies). The d_H of the injected NPT models and the initial sand column signal, as well as 8 mL aliquots of the eluate, were characterized by DLS. Each DLS measurement corresponds to an average of six measurements of 60 seconds ~~each~~. Each sample was assigned a z-average hydrodynamic diameter (d_{zH}) using the cumulant algorithm. Additionally, the Sparse Bayesian learning (SBL) algorithm provides a multimodal analysis to determine the

presence of several d_H (see supplemental information, Figure S1). TEM images were obtained by a Jeol 2100 High Resolution Microscope (Figure S2). Data was analyzed with ImageJ software and the NanoDefine plugin to obtain the area equivalent diameters and the aspect ratios (length of major axis/length of minor axis), presented in Table 1 (Verleysen et al., 2019).

2.4 Transport in porous media

Transport and deposition were studied in a lab-scale sand-packed column using a liquid chromatography system (Äkta™ Pure by General Electric Healthcare). This porous media was composed of Fontainebleau sand (type NE34) with a median diameter (d_{50}) of 210 µm and a uniformity index d_{60}/d_{10} of 1.4. The sand was dry-packed into a borosilicate column (XK 26, GE Healthcare, i.d. = 2.6 cm). The packed bed height varied from 11.2 to 12.7 cm. The porosity was 0.40 ± 0.01 on average. The eluent (mobile phase) was composed of NaCl at 5.0 10^{-3} M. The pH value was fixed at 6.5 using NaOH and HCl. The sand was washed with at least 14 pore volumes (PVs) of deionized water and 22 PVs of the eluent. The pore volume was determined by an injection of NaCl at 5.0 10^{-3} M. Complete tracer tests were performed with KBr. All reactants were analytical grade. The particles and tracers were injected during 6 PVs at a fixed rate of 1.57 10^{-5} $m.s^{-1}$, followed by at least six pore volumes of the plastic-free suspension at the same ionic strength and pH value.

At the outlet, the concentration of the NPT models eluted from the porous media was continuously measured by the UV-Vis spectrophotometer paired to the chromatography system at a wavelength λ = 226 nm, where polystyrene absorption is maximal. Breakthrough curves (BTC) were obtained by plotting the outflowing concentration of the NPT models normalized by the initial concentration as a function of pore volumes eluted. Duplicate experiments were performed for *PSL COOH 200* and *PSL COOH 430-P*. Due to the limited yield of *NPT-P* dispersions and to the variability in size distributions of different *NPT-P* batches, duplicates were not performed.

2.5 Theory

2.5.1 Colloid Filtration Theory (CFT)

Colloid filtration theory (CFT) is used to separate hydrodynamic processes from surface interactions that are occurring in the sand column. It is summarized by equation (1), which expresses the porous media's capacity to trap colloids. The single-collector removal efficiency (η) is the product of the single-collector contact efficiency (η_0) and the attachment efficiency of the particles (α) (Petosa et al., 2010).

$$\eta = \eta_0 \, \alpha \tag{1}$$

The single-collector contact efficiency (η_0) is the capacity of colloids to be trapped by porous media due only to hydrodynamic mechanisms, without any favorable physicochemical conditions. It depends upon a number of factors, including the diameter of the colloids, the diameter of the sand grains in the porous media, the porosity of the sand column, and the flow rate. It was calculated according to the equation developed by Tufenkji and Elimelech (2004). The attachment efficiency (α) is a function of the physicochemical properties of the colloid dispersion and of the sand grain surfaces, such as ionic strength, surface charge and the Hamaker constant of the system. The attachment efficiency (α) is obtained according to equation (2):

$$\alpha = -\frac{2\, d_{50}}{3\,(1-\varepsilon)\eta_0 L} \ln(C/C_0) \tag{2}$$

where d_{50} is the median diameter of the sand grains, ε and L are the sand column porosity and length, respectively, and (C/C_0) is the height of the breakthrough curve.

2.5.1 DLVO theory of colloidal stability

Surface energetics between particles and an infinite flat plane were modeled by the Derjaguin-Landau-Verwey-Overbeek (DLVO) theory, such as the total energy of interaction G^{tot} as the sum of the Lifshitz-van der Waals G^{LW} attraction and the repulsion due to the electronic double layer G^{el}. DLVO theory can be expanded upon and modified to take into account the effect of hydrophobicity, roughness and particle shape, separately. First an extended version of the DLVO theory (XDLVO)

was also modeled by adding the Lewis acid-base (hydrophopic) component G^{AB} to the total energy of interaction. Secondly, the effect of particle shape and orientation was studied thanks to the surface element integration (SEI) method, since is what sets apart *PSL COOH 430-P* and both *NPT-P* particles.

The Lifshitz–van der Waals component G^{LW} of the free energy of interaction between a colloid and a surface is given by:

$$G^{LW} = -\frac{H}{6}\left[\frac{2d_p(h+d_p)}{h(h+2d_p)} - Ln\frac{h+2d_p}{h}\right] \quad (3)$$

where H is the Hamaker constant for the polystyrene-silica-water system, h is the separation distance between the colloid and the sand, and d_p is the radius of the colloid. A Hamaker constant of $1.45\ 10^{-20}$ was calculated from Israelachvili (Israelachvili, 2015) for the interaction between quartz, water and polystyrene.

The electronic double layer component G^{el} is given by:

$$G^{el} = \pi\varepsilon d_p(\zeta_N^2 + \zeta_S^2)\left[\frac{2\zeta_N\zeta_S}{\zeta_N^2+\zeta_S^2}.Ln\frac{1+\exp(-\kappa h)}{1-\exp(-\kappa h)} + Ln\{1-\exp(-2\kappa h)\}\right. \quad (4)$$

where ζ_N and ζ_S are the surface charges of the plastic colloids and of the sand surface, respectively. The zeta potential was used instead of the surface potential. κ is the double layer thickness, which is determined by the following equation:

$$\kappa = \left[\frac{e^2}{\varepsilon k_B T}\sum i z_i n_i\right]^2 \quad (5)$$

where e is the charge of the electron; ε is the permittivity of the medium, which is equal to $6.95\ 10^{-10}$ $C^2.J^{-1}.m^{-1}$, k_B the Boltzmann constant, T the temperature, z_i the valency of the ions i, and n_i the number of ions i per unit volume.

The Lewis acid-base energy of interaction G^{AB} of our system is:

$$G^{AB} = \pi r d_p \lambda \Delta G^{AB} e^{[(h_o-h)/\lambda]} \quad (6)$$

where λ is the correlation length, chosen as 1.65 nm, according to Valsesia et al. (2018), and h_0 is the minimum distance of separation between the particle and the surface, taken as 0.158 nm. The acid-base potential ΔG^{AB} is expressed as:

$$\Delta G^{AB} = -2\left(\sqrt{\gamma_N^{AB}} - \sqrt{\gamma_W^{AB}}\right).\left(\sqrt{\gamma_S^{AB}} - \sqrt{\gamma_W^{AB}}\right)$$

with $\sqrt{\gamma^{AB}}$ referring to the polar component of the surface free energy for W = water, S = sand surface and N = NPT model. $\sqrt{\gamma_W^{AB}}$ is 51.00 mJ.m^{-2} and $\sqrt{\gamma_S^{AB}}$ is 15.00 mJ.m^{-2} according to Barhoumi et al. (Barhoumi et al., 2010).. The polar component of the free energy was measured according the method of Valsesia et al. (2018) for each of the three types of NPT models. $\sqrt{\gamma_N^{AB}}$ values of 33.91, 37.47 and 31.82 mJ.m^{-2} were obtained for *PSL COOH 200*, *PSL COOH 430-P* and *NPT-P*, respectively.

The DLVO theory was modified by the SEI method described by Wu et al. (2013) to understand the effect of *NPT-P*'s nonspherical shape and their different orientations, described by the angle φ that is formed between the major axis of the particle and the collector surface (Bhattacharjee et al., 2000). The interaction energy between a plane surface (collector) and a curved object (particle) were calculated by integrating this energy over the exact surface geometry of the object. Our particles were considered to be rod-like. The semi-major axis (L) and semi-minor axis (a) were determined according to the aspect ratio and the d_{zH} presented in Table 1.

3. Results & Discussion

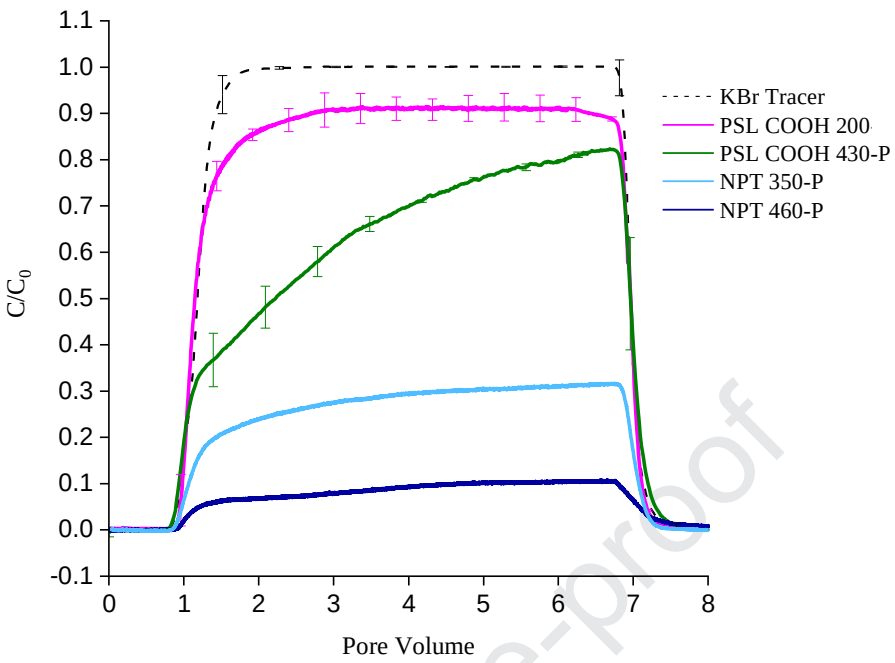

Figure 1: Breakthrough curves of KCl tracer and nanoplastic models injected continuously for 6 pore volumes at an initial concentration (C_0) of 5.0 10^{-3} g.L^{-1} in 5.0 10^{-3} M NaCl and pH 6.5 (error bars = standard deviation, n = 2).

Figure 1 illustrates the breakthrough curves (BTC) of the different NPT models after transport through a sand column at a constant flow rate. Reproducible results are obtained with this experimental setup, as shown by the error bars on the duplicate experiments of *PSL COOH 200* and *PSL COOH 430-P*. A KBr salt tracer shows only the effect of transport by advection and dispersion due to the absence of deposition (C/C_0 of unity). *PSL COOH 200* presents a BTC similar in shape to KBr with 92±5% recovered in column effluent. This result indicates transport through the column with negligible deposition onto the sand. However, 67±1% of *PSL COOH 430-P* are recovered in column effluent, which indicates some deposition occurred. Finally, both polymorphic PS models (*NPT-P*) are the most deposited, with only 28% of *NPT 350-P*, and 10% of *NPT 460-P* that are recovered in column effluent. These results indicate that an increase in particle size causes an increase in the deposition rate. Indeed, when comparing NPT models of similar shape, larger particles are less recovered in column effluent: *PSL COOH 430-P* vs *PSL COOH 200* and *NPT 460-P* vs *NPT 350-P*. The higher transport rate of *PSL COOH 200* compared to *PSL COOH 430-P* may also be due to the

presence of surfactants used for commercial *PSL COOH-200*. Such molecules can enhance nanoparticle transport by decreasing adsorption in the secondary energetic minimum (see DLVO section below) (Tufenkji and Elimelech, 2005). Finally, the absence of a tailing at the end of the BTCs shows that deposited particles did not detach from the porous media (Bradford et al., 2002).

Based on the BTCs, it appears that the particle shape strongly increases the deposition rate in the porous media under dynamic conditions. Surprisingly, *NPT 350-P* is significantly more deposited in porous media than *PSL COOH 430-P*, although they have a smaller initial hydrodynamic diameter and area equivalent diameter (Table 1). This confirms that the asymmetrical and irregular shape of the NPT model (*NPT-P*) significantly increases deposition in the porous media. It should be noted that these experiments were performed at equivalent mass concentrations instead of equivalent particle concentrations. This method was chosen to obtain a quality DLS signal at the outlet of the sand column since light scattering is proportional to the particle diameter. However, it creates a bias that favors elution of the smaller, more numerous particles (Table 1) (Bradford and Bettahar, 2006). Despite this, *NPT 350-P*, which has a higher particle concentration, was more deposited than *PSL COOH 430-P*. This highlights the fact that an irregular asymmetrical shape has a greater impact on the deposition rate than that of size and particle concentration.

To investigate the retention mechanisms of these NPT models, both colloidal filtration theory (CFT) and various Derjaguin-Landau-Verwey-Overbeek (DLVO) theories were studied. According to the CFT, the single-collector contact efficiency (η_0) increases as sub-micrometric particle sizes decrease (Tufenkji and Elimelech, 2004). Hence, smaller particles should be more easily retained, which is not the case in the present study. This suggests that nanoplastic models used here have considerable differences in attachment efficiency (α) and non-classical mechanisms of particle collision are operating. The attachment efficiency (α) obtained by CFT, can be used to compare the affinity of particles with sand across different experimental conditions. Caution must be taken in interpreting α since the CFT is meant to study monodisperse and spherical particles and collectors. Since the sand grains are not monodisperse (d_{60}/d_{10} of 1.4) and nanoplastic models have different degrees of polydispersity (see Table 1), an average α range, named $\overline{\alpha}$, and a range of α were presented

in Table 2 with the corresponding heat-maps presented in supplementary information (Figure S3). An $\overline{\alpha}$ of 0.0034 ± 0.0005 was obtained for *PSL COOH 200*, whereas *PSL COOH 430-P* had an $\overline{\alpha}$ = 0.012 ± 0.0008 (Table 2). These results are in agreement with other studies, such as Bradford et al. (2002), who found that the 450 nm carboxylated PSL attachment efficiency in 10^{-3} M KCl at pH 6.8 varied from α = 0.0037 to α = 0.014 according to the polydispersity and average grain size of the quartz sand (Bradford et al., 2002). Tufenkji and Elimelech (2005) found α values of 0.0058 and 0.014 for 320 nm PSL COOH in 20 10^{-3} M KCl at pH 8. For the polymorphic NPT models, the average attachment efficiency is one order of magnitude greater than that for the spherical models, with α = 0.069 for *NPT 350-P* and 0.14 for *NPT 460-P*. This large increase in attachment efficiency is more likely to represent different hydrodynamic flow processes than a change in surface affinity. Indeed, the CFT theory is unsuitable to study the flow of nonspherical particles and largely overestimates α (and underestimates η_0) when the particle shape deviates from that of a sphere (Salerno et al., 2006).

Table 2: Summary of the percent in column effluent and attachment efficiencies (α) for the different nanoplastic models. The attachment efficiencies are based on average particle diameter (d_p) and collector diameters (d_c) and a range of dp and dc equal to the standard deviation (σ) of the size distributions. (Error bars = standard deviation of the duplicate experiments).

Nanoplastic Model	**Percent in Column Effluent (%)**	**Attachment Efficiency (α)**		
		dp – σ and dc - σ	**Average dp and dc**	**dp + σ and dc + σ**
PSL COOH 200	92 ± 5	$2.0\ 10^{-3} \pm 0.4\ 10^{-3}$	$3.4\ 10^{-3} \pm 0.5\ 10^{-3}$	$5.4\ 10^{-3} \pm 1.1\ 10^{-3}$
PSL COOH 430-P	67 ± 1	$6.9\ 10^{-3} \pm 0.8\ 10^{-3}$	$1.2\ 10^{-2} \pm 0.1\ 10^{-2}$	$1.9\ 10^{-2} \pm 0.2\ 10^{-2}$
NPT 350-P	28	$4.0\ 10^{-2}$	$6.9\ 10^{-2}$	$1.2\ 10^{-1}$
NPT 460-P	10	$7.9\ 10^{-2}$	$1.4\ 10^{-1}$	$2.5\ 10^{-1}$

Since the attachment efficiencies (α) obtained by the CFT theory should only reflect surface energetic interactions, they can be compared with the profiles of the interaction energy between the particles and the sand. Total surface energetic interactions (G^{tot}) are modeled according to DLVO theory by taking the sum of the Lifshitz-van der Waals attraction (G^{LW}) and the repulsion due to the

electronic double layer (G^{el}). An extended version, the XDLVO theory, includes the Lewis acid-base (hydrophobic) interaction energy (G^{AB}). This component has been carefully quantified using the method described by Valsesia et al. (2018). It should be noted, however, that since DLVO and XDLVO theories assume that the particles are spherical, they cannot correctly determine the interaction energy of the asymmetrical and irregularly shaped *NPT-P*s (Hotze et al., 2010). To overcome this limitation, a SEI-modified DLVO calculates G^{LW} and G^{el} between an elongated particle and the sand surface. This modified DLVO does not, however, incorporate the hydrophobic component of the interaction energy. It is important to note that in these experimental conditions, advection prevails over diffusion, with a Peclet number varying from 112 to 240 for *PSL COOH 200* and *NPT 460-P*, respectively. In these conditions, particle deposition can occur if the adhesive forces are stronger than the hydrodynamic forces. Therefore, the objective is only to investigate whether the physical and chemical properties of the particles modeled by the different DLVO theories, are correlated to the attachment efficiencies in the sand column and hence a good predictor of adhesive forces. Surface energetic interactions should not be considered an absolute prediction of deposition behavior. If the energy of interaction predicts trends in transport, the most transported particles should have the highest energetic barrier to deposition (ΔG^{tot}_{max}) and lowest secondary energetic minimum (ΔG^{tot}_{min2}), where reversible deposition can occur.

Table 3: Summary of primary maximum (ΔG^{tot}_{max}) and secondary energetic minimum (ΔG^{tot}_{min2}) of interaction energies according to DLVO, SEI -modified DLVO and XDLVO theories, for the different nanoplastic models.

	DLVO Theory		SEI-modified DLVO Theory				XDLVO Theory	
			φ = 0 radians		φ = π/3 radians			
Nanoplastic Model	**ΔG^{tot}_{max} (k_BT)**	**ΔG^{tot}_{min2} (k_BT)**	**ΔG^{tot}_{max} (k_BT)**	**ΔG^{tot}_{min2} (k_BT)**	**ΔG^{tot}_{max} (k_BT)**	**ΔG^{tot}_{min2} (k_BT)**	**ΔG^{tot}_{max} (k_BT)**	**ΔG^{tot}_{min2} (k_BT)**
PSL COOH 200	175	-0.7	-	-	-	-	51	-0.7
PSL COOH 430-P	235	-2.2	-	-	-	-	74	-2.0
NPT 350-P	244	-1.6	$4.5\ 10^{10}$	-0.4	45	-1.5	64	-1.6
NPT 460-P	321	-2.3	$5.9\ 10^{10}$	-0.4	52	-1.8	83	-2.3

According to DLVO theory, all particles undergo significant repulsion from the sand grains, with ΔG^{tot}_{max} equal to 175 k_BT for *PSL COOH 200*, 235 k_BT for *PSL COOH 430-P*, 244 k_BT for *NPT 350-P*, and 321 k_BT for *NPT 460-P* (Table 3 and full lines in Figure 2a). Based on the energy profiles, no colloid can overcome the energy barrier (ΔG^{tot}_{max}) and irreversibly deposit in the primary minimum (ΔG^{tot}_{min1}). The secondary energetic minimum (ΔG^{tot}_{min2}) occurs between 20 and 60 nm from the sand surface. It varies from as low as -2.3 k_BT for *NPT 460-P*, -2.2 k_BT for *PSL COOH 430-P*, -1.6 k_BT for *NPT 460-P* to -0.7 k_BT for *PSL COOH 200* (Table 3 and full lines in Figure 2c). For the three larger particles, reversible retention in the secondary energetic minimum can occur since the depth is larger than 1.5 k_BT, which is the thermal energy of diffusion (Israelachvili, 2015).

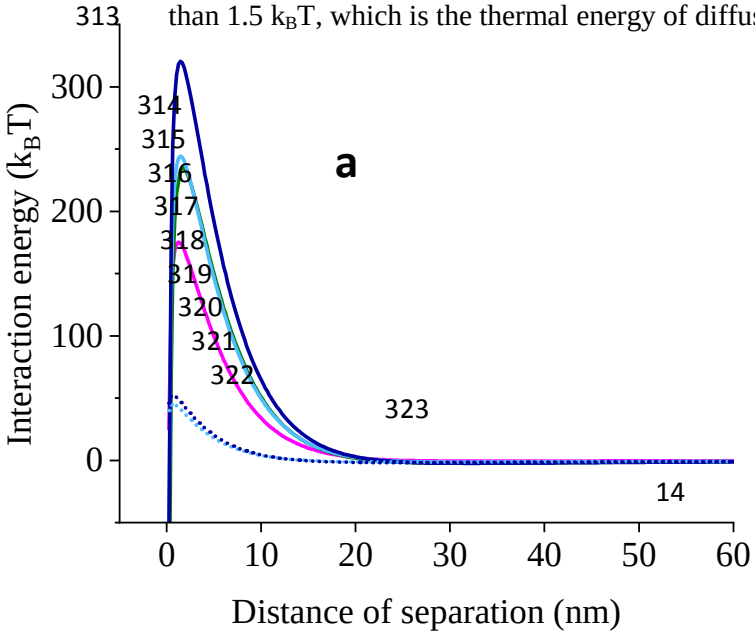

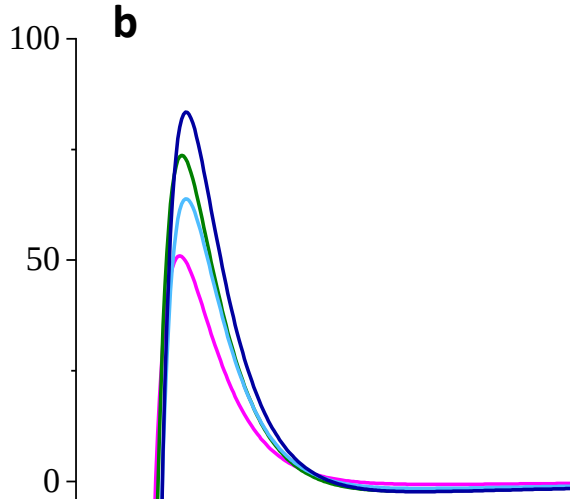

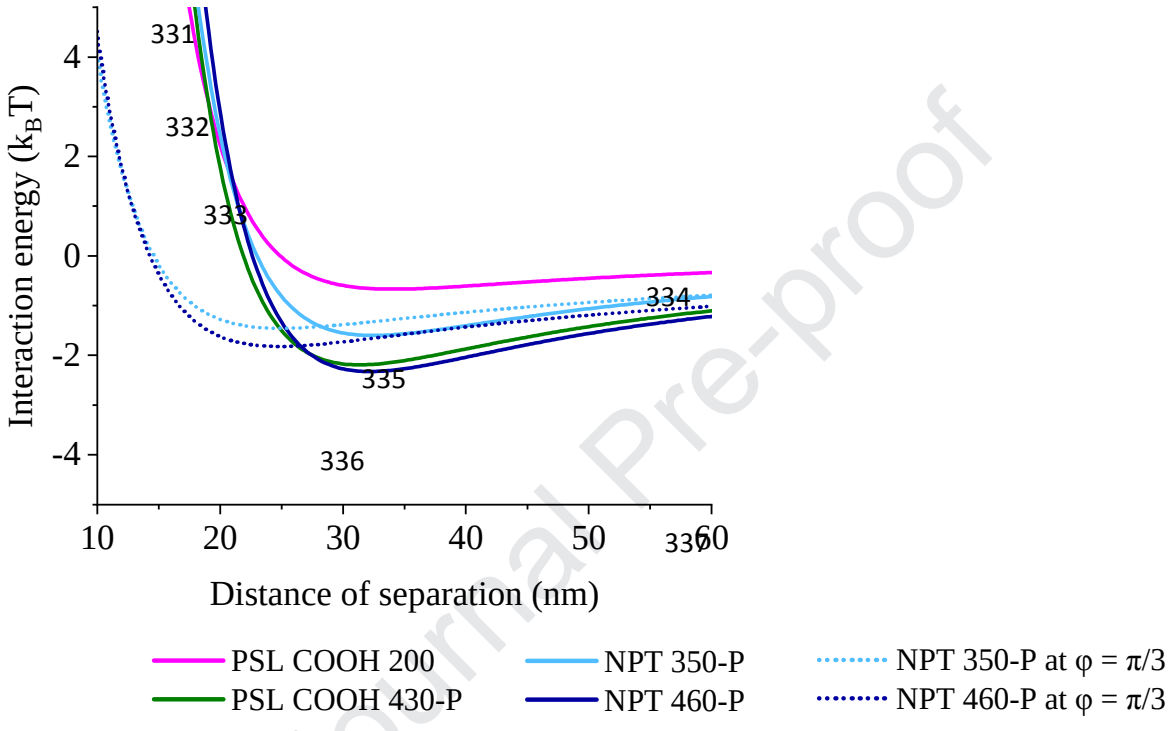

Figure 2: Interaction energy, scaled to k_BT, between the nanoplastic models and the sand grain collector as a function of distance according to a) DLVO theory (full lines) and SEI -modified DLVO theory (dashed lines) and b) XDLVO theory. The identical data is replotted in c) and d) to highlight the secondary energetic minimum of panels a) and b) respectively.

By accounting for the polar component of the interaction energy, the XDLVO theory predicts similar global trends but indicates a much lower repulsion of all particles from the sand surface (Figures 2b and 2d). The maximum heights of ΔG^{tot}_{max} for spherical particles *PSL COOH 200* and *PSL COOH 430-P* are equal to 51 k_BT and 74 k_BT, respectively. For the asymmetrical and irregularly shaped particles, ΔG^{tot}_{max} is comparable: 64 k_BT and 83 k_BT for *NPT 350-P* and *NPT 460-P*, respectively (Table 3 and Figure 2b). Based on the height of the energy barriers, still no colloid

deposition should occur in the primary minima. The depth of the secondary energetic minimum (ΔG^{tot}_{min2}) is unchanged compared to that determined by the DLVO theory (Table 3 and Figure 2d).

The dashed lines in Figures 2a and 2c show the minimal interaction energy between the sand surface and the *NPT-P* models, according to the SEI-modified DLVO theory. This occurs when they form an angle (φ) of $\pi/3$ with the collector surface (Gomez-Flores et al., 2019). ΔG^{tot}_{max} is reduced to 45 k_BT and 52 k_BT for *NPT 350-P* and *NPT 460-P*, respectively (Table 3). The interaction energy is maximal at $\varphi = 0$ (Table 3 and Figure S4). This is mostly due to the fact the particle surface is closer to the collector (Gomez-Flores et al., 2019). ΔG^{tot}_{min2} is only slightly less deep than predicted by DLVO and XDLVO theories (Table 3 and Figure 2c).

The high retention rate of the *NPT-P* particles can be in part attributed to the fact that they may find orientations where there is no energy barrier to irreversible deposition (ΔG^{tot}_{min1}) (Gomez-Flores et al., 2019). This can be expected to occur when both particle orientation and hydrophobicity are accounted for simultaneously. Furthermore, the magnitude of the total energies of interaction (ΔG^{tot}) of *PSL COOH 430-P, NPT 350-P* and *NPT 460-P*s and the sand surfaces may be overestimated by the all DLVO models due to their surface roughness (Table 1 and Figure S2) (Bhattacharjee et al., 1998; Hoek and Agarwal, 2006). *NPT-P* particles are characterized by a large range of orientation-dependent interaction energies (Table 3 and S5), which will give them considerable torque. This added torque can provide the particles sufficient kinetic energy to overcome an energy barrier (ΔG^{tot}_{max}) that is significantly reduced at some orientations Figure 2a (Seymour et al., 2013).

However, the DLVO and XDLVO theories are inadequate to predict the deposition of plastic nanoparticles in porous media. On the one hand, the DLVO and XDLVO theories globally underestimate the amount of deposition that particles undergo. This is a well-known effect when studying the transport of particles in unfavorable (repulsive) conditions (Elimelech and O'Melia, 1990). On the other hand, the height of the energy barrier is not proportional to the level of repulsion, nor is the depth of the secondary energetic minimum proportional to the level of deposition. For example, *PSL COOH 200* is the most transported particle, although it has the lowest energy barrier (ΔG^{tot}_{max}). This occurs because all interaction energies scale linearly with particle size (Elimelech and

O'Melia, 1990). In other words, larger particles should undergo more repulsion and be more transported, especially since all particles present comparable polar components of the surface free energy (γ^{AB}) and zeta potentials (ζ_N). However, contrary to these DLVO and XDLVO predictions, *NPT 460-P*, which has a higher energy barrier, is more deposited than *NPT 350-P*. Although a high energy barrier is present, particles may be retained by 1) attachment onto chemical heterogeneities on the colloid and collector surfaces that act as favorable sites (Seymour et al., 2013; Tufenkji and Elimelech, 2005) 2) reversible attachment in the secondary energetic minimum (Tufenkji and Elimelech, 2005) and 3) straining (trapping of particles in pore throats that are too small to allow the passage of particles) (Bradford et al., 2002; McDowell-Boyer et al., 1986). Furthermore, pore geometry creates a variety of speed profiles, such that particles may also be retained in zones with a lower flow velocity where the hydrodynamic forces are lowered (Elimelech and O'Melia, 1990). Indeed, pore geometry plays a dominant role in colloid retention under conditions where a high energy barrier exists (Tong and Johnson, 2006).

To determine the extent to which deposition can be attributed to chemical heterogeneity, batch adsorption experiments were conducted. The results, presented in S5, show that none of our plastic nanoparticles are significantly adsorbed onto the sand. While results from batch and column experiments can be difficult to compare when they are not normalized by $\overline{\alpha}$ =1, our batch experiments do show that chemical heterogeneity is far from significative (Geitner et al., 2017; Treumann et al., 2014). This points to the importance of straining and adsorption in the secondary energetic minimum.

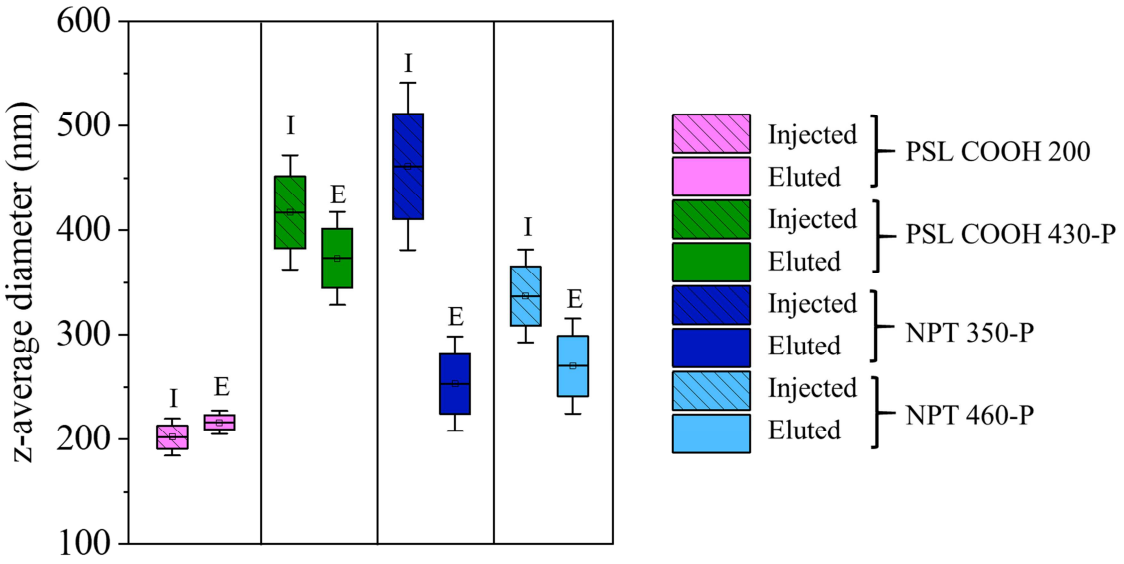

396

397 *Figure 3: z-average hydrodynamic diameters (d_{zH}) of the plastic nanoparticles before and after flowing through the sand*
398 *column (n=6, error bars= standard deviation).*

399 The evolution of the hydrodynamic diameters of the particles injected in and eluted from
400 through the porous media can also indicate what processes occur in the column (Figure 3). The
401 average size and polydispersity of eluted particles were constant during elution. The average
402 hydrodynamic diameters (d_{zH}) of the smaller spheres, *PSL COOH 200*, do not change significantly
403 (+4%). The larger spherical particles, *PSL COOH 430-P*, undergo a more pronounced decrease in d_{zH}
404 after flowing through the sand column (-11%). Both spherical particles' polydispersities do not vary
405 significantly. For the asymmetrical NPT models, the decrease in d_{zH} after elution is globally greater
406 and even more pronounced for the larger particles (-45% for *NPT 460-P*) compared to that of the
407 smaller particles
408 (-20% for *NPT 350-P*). The smaller size fraction of irregularly shaped particles, approximately 200 nm
409 in diameter, is most mobile in the sand column. Furthermore, the polydispersity of the samples
410 containing asymmetrical and irregular particles decreases. These changes in size point to a mechanism
411 of physical retention of spherical particles larger than 380 nm and irregularly shaped particles larger
412 than approximately 200 nm. This confirms that large particles are deposited by physical straining in
413 the pores of the sand column, which is unaccounted for by the DLVO theories and underestimated by

CFT (Bradford et al., 2002). In similar experimental conditions, Weiss et al. (Weiss et al., 1995) noted a similar effect concerning the transport of 14 different bacterial strains. The bacterial cells recovered in the eluent were not only smaller but also rounder than the cells injected.

The deposition rate increases as the particle size increases and as its shape deviates from that of a sphere. In other words, smaller and smoother particles are more easily transported. This can be partially attributed to straining. Straining is expected to start having an effect when the ratio of the particle radius to the median collector radius (d_p/d_{50}) exceeds 0.0017 (Bradford et al., 2002). This is satisfied in the case of *PSL COOH 430-P* (d_p/d_{50} = 0.002). Concerning *NPT-Ps*, since most particles larger than approximately 200 nm are retained, straining occurs at a lower d_p/d_{50} ratio (Figure 3). Straining of these particles is enhanced because the hydrodynamics of nonspherical particle flow in porous media are more complex than those of spherical particles. In highly repulsive conditions (thousands of k_BT), elongated particles and are not more deposited than spherical particles since they can orient their major axis parallel to the flow (Xu et al., 2008). However, in our conditions, where there is less repulsion (10s of k_BT) nonspherical particles are increasingly deposited. This is attributed to larger collision frequencies with the porous media (Salerno et al., 2006). The CFT underestimates the single-collector contact efficiency (η_0) for spheroidal particles (Salerno et al., 2006). Finally, the *NPT-P* dispersions are highly polydisperse and as such will contain a higher fraction of large particles that are likely to be retained.

As mentioned above, reversible deposition in the secondary energetic minimum is possible for *PSL COOH 430-P* and both polymorphic particles *NPT 350-P* and *NPT 460-P*. The asymmetrical BTC shape of the *PSL COOH 430-P* is typical of either particle release from the secondary energetic minimum or blocking of the flowing particles by previously deposited particles (Bradford et al., 2002; Bradford and Bettahar, 2006; Redman et al., 2004; Tufenkji and Elimelech, 2005). This was not observed for *NPT 350-P* and *NPT 460-P*, whose BTCs instead reach a plateau. It indicates either that the asymmetrical models are not detached and undergoing re-entrainment from the sand or that deposited particles do not block the incoming particles. Colloidal detachment and re-entrainment from the secondary energetic minimum mostly occur by rolling, which is easiest for spherical particles.

Despite the fact that nonspherical particles have larger hydrodynamic torques than spherical particles, as particles deviate from an ideal spherical shape, they present a higher moment arm requiring more energy to induce rolling (Bergendahl and Grasso, 2000; Seymour et al., 2013) The flat BTC may also indicate that deposited particles create more favorable sites for deposition by increasing the physical roughness of the porous media (Seymour et al., 2013). Finally, the shape of the *NPT-P*'s BTCs suggest that reversible deposition not be as dominant a mechanism as straining and deposition in the primary energetic minimum.

4. Conclusion

This study showed that the physicochemical properties of the NPT models significantly affect their propensity to be transported. The asymmetrical and irregular shape of the environmentally relevant NPT model has a strikingly positive impact on the deposition rate in the sand column compared to that impact of particle size, composition or concentration. The deposition of these models in the porous media may be attributed partially to physical retention, as witnessed by the straining of the larger size fractions. Their deposition is also attributed to an orientation-dependent level of repulsion (ΔG^{tot}_{max}) which allows the particles to take on the most thermodynamically preferable orientation, and possibly to overcome the energy barrier to irreversible deposition (ΔG^{tot}_{max}), given sufficient hydodynamic torque. These results point to the importance of choosing environmentally relevant NPT models. Their asymmetrical and irregular shape, which is characteristic of the mechanical abrasion of plastic debris, increases their deposition rate in a sand column by an order of magnitude. It is clear that the relevance of environmental fate studies depends upon the quality of the proxies used (Koelmans, 2019). More particularly, the impact of the NPT composition (polymer type, additives and sorbed contaminants), average size and size distribution as well as NPT shape are crucial parameters to study (Wagner and Reemtsma, 2019).

The importance of the physical and chemical properties of the NPT models has been demonstrated here. Further studies are needed on the one hand, to define single-collector contact efficiency (η_0) for nonspherical particles and to quantify the amount of deposition that can be attributed to straining, irreversible attachment (in ΔG^{tot}_{min1}) and reversible attachment (in ΔG^{tot}_{min2}). On

the other hand, more research is needed to implement these results by taking into account the environmental conditions of the porous media (ionic strength, natural organic matter, pH value, and soil composition). Such a complete approach is needed to fully assess the fate of NPTs in freshwater and terrestrial environments.

Competing Interest Statement

The authors declare that they have no competing interests.

References

Allen, S., Allen, D., Phoenix, V.R., Le Roux, G., Durántez Jiménez, P., Simonneau, A., Binet, S., Galop, D., 2019. Atmospheric transport and deposition of microplastics in a remote mountain catchment. Nature Geoscience. https://doi.org/10.1038/s41561-019-0335-5

Bank, M.S., Hansson, S.V., 2019. The Plastic Cycle: A Novel and Holistic Paradigm for the Anthropocene. Environ. Sci. Technol. acs.est.9b02942. https://doi.org/10.1021/acs.est.9b02942

Barhoumi, H., Maaref, A., Jaffrezic-Renault, N., 2010. Experimental Study of Thermodynamic Surface Characteristics and pH Sensitivity of Silicon Dioxide and Silicon Nitride. Langmuir 26, 7165–7173. https://doi.org/10.1021/la904251m

Bergendahl, J., Grasso, D., 2000. Prediction of colloid detachment in a model porous media: hydrodynamics. Chemical Engineering Science 55, 1523–1532. https://doi.org/10.1016/S0009-2509(99)00422-4

Bhattacharjee, S., Chen, J.Y., Elimelech, M., 2000. DLVO interaction energy between spheroidal particles and a flat surface. Colloids and Surfaces A: Physicochemical and Engineering Aspects 165, 143–156. https://doi.org/10.1016/S0927-7757(99)00448-3

Bhattacharjee, S., Ko, C.-H., Elimelech, M., 1998. DLVO Interaction between Rough Surfaces. Langmuir 14, 3365–3375. https://doi.org/10.1021/la971360b

Bradford, S.A., Bettahar, M., 2006. Concentration dependent transport of colloids in saturated porous media. Journal of Contaminant Hydrology 82, 99–117. https://doi.org/10.1016/j.jconhyd.2005.09.006

Bradford, S.A., Yates, S.R., Bettahar, M., Simunek, J., 2002. Physical factors affecting the transport and fate of colloids in saturated porous media: FACTORS AFFECTING THE FATE OF COLLOIDS. Water Resources Research 38, 63-1-63–12. https://doi.org/10.1029/2002WR001340

Carpenter, E.J., Smith, K.L., 1972. Plastics on the Sargasso Sea Surface. Science 175, 1240–1241. https://doi.org/10.1126/science.175.4027.1240

Carr, S.A., Liu, J., Tesoro, A.G., 2016. Transport and fate of microplastic particles in wastewater treatment plants. Water Research 91, 174–182. https://doi.org/10.1016/j.watres.2016.01.002

Cozar, A., Echevarria, F., Gonzalez-Gordillo, J.I., Irigoien, X., Ubeda, B., Hernandez-Leon, S., Palma, A.T., Navarro, S., Garcia-de-Lomas, J., Ruiz, A., Fernandez-de-Puelles, M.L., Duarte, C.M., 2014. Plastic debris in the open ocean. Proceedings of the National Academy of Sciences 111, 10239–10244. https://doi.org/10.1073/pnas.1314705111

Dong, Z., Zhang, W., Qiu, Y., Yang, Z., Wang, J., Zhang, Y., 2019a. Cotransport of nanoplastics (NPs) with fullerene (C60) in saturated sand: Effect of NPs/C60 ratio and seawater salinity. Water Research 148, 469–478. https://doi.org/10.1016/j.watres.2018.10.071

Dong, Z., Zhu, L., Zhang, W., Huang, R., Lv, X., Jing, X., Yang, Z., Wang, J., Qiu, Y., 2019b. Role of surface functionalities of nanoplastics on their transport in seawater-saturated sea sand. Environmental Pollution 255, 113177. https://doi.org/10.1016/j.envpol.2019.113177

Elimelech, M., O'Melia, C.R., 1990. Effect of particle size on collision efficiency in the deposition of Brownian particles with electrostatic energy barriers. Langmuir 6, 1153–1163. https://doi.org/10.1021/la00096a023

Galloway, T.S., 2015. Micro- and Nano-plastics and Human Health, in: Bergmann, M., Gutow, L., Klages, M. (Eds.), Marine Anthropogenic Litter. Springer International Publishing, Cham, pp. 343–366. https://doi.org/10.1007/978-3-319-16510-3_13

Geitner, N.K., O'Brien, N.J., Turner, A.A., Cummins, E.J., Wiesner, M.R., 2017. Measuring Nanoparticle Attachment Efficiency in Complex Systems. Environmental Science & Technology 51, 13288–13294. https://doi.org/10.1021/acs.est.7b04612

Gewert, B., Plassmann, M.M., MacLeod, M., 2015. Pathways for degradation of plastic polymers floating in the marine environment. Environmental Science: Processes & Impacts 17, 1513–1521. https://doi.org/10.1039/C5EM00207A

Gigault, J., Halle, A. ter, Baudrimont, M., Pascal, P.-Y., Gauffre, F., Phi, T.-L., El Hadri, H., Grassl, B., Reynaud, S., 2018. Current opinion: What is a nanoplastic? Environmental Pollution 235, 1030–1034. https://doi.org/10.1016/j.envpol.2018.01.024

Gigault, J., Pedrono, B., Maxit, B., Halle, A.T., 2016. Marine plastic litter: the unanalyzed nano-fraction. Environ. Sci.: Nano 3, 346–350. https://doi.org/10.1039/C6EN00008H

Gomez-Flores, A., Bradford, S.A., Wu, L., Kim, H., 2019. Interaction energies for hollow and solid cylinders: Role of aspect ratio and particle orientation. Colloids and Surfaces A: Physicochemical and Engineering Aspects 580, 123781. https://doi.org/10.1016/j.colsurfa.2019.123781

Hadri, H.E., Gigault, J., Maxit, B., Grassl, B., Reynaud, S., 2020. Nanoplastic from mechanically degraded primary and secondary microplastics for environmental assessments. NanoImpact 100206. https://doi.org/10.1016/j.impact.2019.100206

Hartmann, N.B., Hüffer, T., Thompson, R.C., Hassellöv, M., Verschoor, A., Daugaard, A.E., Rist, S., Karlsson, T., Brennholt, N., Cole, M., Herrling, M.P., Hess, M.C., Ivleva, N.P., Lusher, A.L., Wagner, M., 2019. Are We Speaking the Same Language? Recommendations for a Definition and Categorization Framework for Plastic Debris. Environ. Sci. Technol. 53, 1039–1047. https://doi.org/10.1021/acs.est.8b05297

He, L., Wu, D., Rong, H., Li, M., Tong, M., Kim, H., 2018. Influence of Nano- and Microplastic Particles on the Transport and Deposition Behaviors of Bacteria in Quartz Sand. Environ. Sci. Technol. acs.est.8b01673. https://doi.org/10.1021/acs.est.8b01673

Hiemenz, P.C., Rajagopalan, Raj., 1997. Principles of colloid and surface chemistry. Dekker, New York; Basel; Hong Kong.

Hoek, E.M.V., Agarwal, G.K., 2006. Extended DLVO interactions between spherical particles and rough surfaces. Journal of Colloid and Interface Science 298, 50–58. https://doi.org/10.1016/j.jcis.2005.12.031

Horton, A.A., Walton, A., Spurgeon, D.J., Lahive, E., Svendsen, C., 2017. Microplastics in freshwater and terrestrial environments: Evaluating the current understanding to identify the knowledge gaps and future research priorities. Science of The Total Environment 586, 127–141. https://doi.org/10.1016/j.scitotenv.2017.01.190

Hotze, E.M., Phenrat, T., Lowry, G.V., 2010. Nanoparticle Aggregation: Challenges to Understanding Transport and Reactivity in the Environment. Journal of Environment Quality 39, 1909. https://doi.org/10.2134/jeq2009.0462

Hu, E., Shang, S., Fu, Z., Zhao, X., Nan, X., Du, Y., Chen, X., 2020. Cotransport of naphthalene with polystyrene nanoplastics (PSNP) in saturated porous media: Effects of PSNP/naphthalene ratio and ionic strength. Chemosphere 245, 125602. https://doi.org/10.1016/j.chemosphere.2019.125602

562 Huerta Lwanga, E., Mendoza Vega, J., Ku Quej, V., Chi, J. de los A., Sanchez del Cid, L., Chi, C.,
563 Escalona Segura, G., Gertsen, H., Salánki, T., van der Ploeg, M., Koelmans, A.A., Geissen, V.,
564 2017. Field evidence for transfer of plastic debris along a terrestrial food chain. Sci Rep 7,
565 14071. https://doi.org/10.1038/s41598-017-14588-2
566 Israelachvili, J.N., 2015. Intermolecular and surface forces.
567 Jambeck, J.R., Geyer, R., Wilcox, C., Siegler, T.R., Perryman, M., Andrady, A., Narayan, R., Law, K.L.,
568 2015. Plastic waste inputs from land into the ocean. Science 347, 768–771.
569 https://doi.org/10.1126/science.1260352
570 Jamieson, A.J., Malkocs, T., Piertney, S.B., Fujii, T., Zhang, Z., 2017. Bioaccumulation of persistent
571 organic pollutants in the deepest ocean fauna. Nat Ecol Evol 1, 51.
572 https://doi.org/10.1038/s41559-016-0051
573 Koelmans, A.A., 2019. Proxies for nanoplastic. Nature Nanotechnology 14, 307–308.
574 https://doi.org/10.1038/s41565-019-0416-z
575 Koelmans, Albert A., Besseling, E., Foekema, E., Kooi, M., Mintenig, S., Ossendorp, B.C., Redondo-
576 Hasselerharm, P.E., Verschoor, A., van Wezel, A.P., Scheffer, M., 2017. Risks of Plastic Debris:
577 Unravelling Fact, Opinion, Perception, and Belief. Environ. Sci. Technol. 51, 11513–11519.
578 https://doi.org/10.1021/acs.est.7b02219
579 Koelmans, Albert A, Kooi, M., Law, K.L., van Sebille, E., 2017. All is not lost: deriving a top-down mass
580 budget of plastic at sea. Environmental Research Letters 12, 114028.
581 https://doi.org/10.1088/1748-9326/aa9500
582 Lambert, S., Wagner, M., 2016. Characterisation of nanoplastics during the degradation of
583 polystyrene. Chemosphere 145, 265–268.
584 https://doi.org/10.1016/j.chemosphere.2015.11.078
585 Law, K.L., Moret-Ferguson, S., Maximenko, N.A., Proskurowski, G., Peacock, E.E., Hafner, J., Reddy,
586 C.M., 2010. Plastic Accumulation in the North Atlantic Subtropical Gyre. Science 329, 1185–
587 1188. https://doi.org/10.1126/science.1192321
588 Lecoanet, H.F., Bottero, J.-Y., Wiesner, M.R., 2004. Laboratory Assessment of the Mobility of
589 Nanomaterials in Porous Media. Environmental Science & Technology 38, 5164–5169.
590 https://doi.org/10.1021/es0352303
591 Lehner, R., Weder, C., Petri-Fink, A., Rothen-Rutishauser, B., 2019. Emergence of Nanoplastic in the
592 Environment and Possible Impact on Human Health. Environmental Science & Technology.
593 https://doi.org/10.1021/acs.est.8b05512
594 Liu, J., Zhang, T., Tian, L., Liu, X., Qi, Z., Ma, Y., Ji, R., Chen, W., 2019. Aging Significantly Affects
595 Mobility and Contaminant-mobilizing Ability of Nanoplastics in Saturated Loamy Sand.
596 Environ. Sci. Technol. acs.est.9b00787. https://doi.org/10.1021/acs.est.9b00787
597 McDowell-Boyer, L.M., Hunt, J.R., Sitar, N., 1986. Particle transport through porous media. Water
598 Resour. Res. 22, 1901–1921. https://doi.org/10.1029/WR022i013p01901
599 Ng, E.-L., Huerta Lwanga, E., Eldridge, S.M., Johnston, P., Hu, H.-W., Geissen, V., Chen, D., 2018. An
600 overview of microplastic and nanoplastic pollution in agroecosystems. Science of The Total
601 Environment 627, 1377–1388. https://doi.org/10.1016/j.scitotenv.2018.01.341
602 Obbard, R.W., Sadri, S., Wong, Y.Q., Khitun, A.A., Baker, I., Thompson, R.C., 2014. Global warming
603 releases microplastic legacy frozen in Arctic Sea ice. Earth's Future 2, 315–320.
604 https://doi.org/10.1002/2014EF000240
605 Pelley, A.J., Tufenkji, N., 2008. Effect of particle size and natural organic matter on the migration of
606 nano- and microscale latex particles in saturated porous media. Journal of Colloid and
607 Interface Science 321, 74–83. https://doi.org/10.1016/j.jcis.2008.01.046
608 Peng, G., Bellerby, R., Zhang, F., Sun, X., Li, D., 2020. The ocean's ultimate trashcan: Hadal trenches as
609 major depositories for plastic pollution. Water Research 168, 115121.
610 https://doi.org/10.1016/j.watres.2019.115121
611 Pessoni, L., Veclin, C., El Hadri, H., Cugnet, C., Davranche, M., Pierson-Wickmann, A.-C., Gigault, J.,
612 Grassl, B., Reynaud, S., 2019. Soap- and metal-free polystyrene latex particles as a
613 nanoplastic model. Environ. Sci.: Nano 6, 2253–2258. https://doi.org/10.1039/C9EN00384C

Petosa, A.R., Jaisi, D.P., Quevedo, I.R., Elimelech, M., Tufenkji, N., 2010. Aggregation and Deposition of Engineered Nanomaterials in Aquatic Environments: Role of Physicochemical Interactions. Environmental Science & Technology 44, 6532–6549. https://doi.org/10.1021/es100598h

Quevedo, I.R., Tufenkji, N., 2012. Mobility of Functionalized Quantum Dots and a Model Polystyrene Nanoparticle in Saturated Quartz Sand and Loamy Sand. Environmental Science & Technology 46, 4449–4457. https://doi.org/10.1021/es2045458

Redman, J.A., Walker, S.L., Elimelech, M., 2004. Bacterial Adhesion and Transport in Porous Media: Role of the Secondary Energy Minimum. Environ. Sci. Technol. 38, 1777–1785. https://doi.org/10.1021/es034887l

Rillig, M.C., 2012. Microplastic in Terrestrial Ecosystems and the Soil? Environmental Science & Technology 46, 6453–6454. https://doi.org/10.1021/es302011r

Salerno, M.B., Flamm, M., Logan, B.E., Velegol, D., 2006. Transport of Rodlike Colloids through Packed Beds. Environ. Sci. Technol. 40, 6336–6340. https://doi.org/10.1021/es0614565

Scheurer, M., Bigalke, M., 2018. Microplastics in Swiss Floodplain Soils. Environ. Sci. Technol. 52, 3591–3598. https://doi.org/10.1021/acs.est.7b06003

Schwarz, A.E., Ligthart, T.N., Boukris, E., van Harmelen, T., 2019. Sources, transport, and accumulation of different types of plastic litter in aquatic environments: A review study. Marine Pollution Bulletin 143, 92–100. https://doi.org/10.1016/j.marpolbul.2019.04.029

Seymour, M.B., Chen, G., Su, C., Li, Y., 2013. Transport and Retention of Colloids in Porous Media: Does Shape Really Matter? Environ. Sci. Technol. 130722083052008. https://doi.org/10.1021/es4016124

Syngouna, V.I., Chrysikopoulos, C.V., 2013. Cotransport of clay colloids and viruses in water saturated porous media. Colloids and Surfaces A: Physicochemical and Engineering Aspects 416, 56–65. https://doi.org/10.1016/j.colsurfa.2012.10.018

Ter Halle, A., Jeanneau, L., Martignac, M., Jardé, E., Pedrono, B., Brach, L., Gigault, J., 2017. Nanoplastic in the North Atlantic Subtropical Gyre. Environmental Science & Technology 51, 13689–13697. https://doi.org/10.1021/acs.est.7b03667

Tong, M., Johnson, W.P., 2006. Excess Colloid Retention in Porous Media as a Function of Colloid Size, Fluid Velocity, and Grain Angularity. Environ. Sci. Technol. 40, 7725–7731. https://doi.org/10.1021/es061201r

Treumann, S., Torkzaban, S., Bradford, S.A., Visalakshan, R.M., Page, D., 2014. An explanation for differences in the process of colloid adsorption in batch and column studies. Journal of Contaminant Hydrology 164, 219–229. https://doi.org/10.1016/j.jconhyd.2014.06.007

Tufenkji, N., Elimelech, M., 2005. Breakdown of Colloid Filtration Theory: Role of the Secondary Energy Minimum and Surface Charge Heterogeneities. Langmuir 21, 841–852. https://doi.org/10.1021/la048102g

Tufenkji, N., Elimelech, M., 2004. Correlation Equation for Predicting Single-Collector Efficiency in Physicochemical Filtration in Saturated Porous Media. Environmental Science & Technology 38, 529–536. https://doi.org/10.1021/es034049r

Valsesia, A., Desmet, C., Ojea-Jiménez, I., Oddo, A., Capomaccio, R., Rossi, F., Colpo, P., 2018. Direct quantification of nanoparticle surface hydrophobicity. Commun Chem 1, 53. https://doi.org/10.1038/s42004-018-0054-7

van Sebille, E., Wilcox, C., Lebreton, L., Maximenko, N., Hardesty, B.D., van Franeker, J.A., Eriksen, M., Siegel, D., Galgani, F., Law, K.L., 2015. A global inventory of small floating plastic debris. Environmental Research Letters 10, 124006. https://doi.org/10.1088/1748-9326/10/12/124006

Verleysen, E., Wagner, T., Lipinski, H.-G., Kägi, R., Koeber, R., Boix-Sanfeliu, A., De Temmerman, P.-J., Mast, J., 2019. Evaluation of a TEM based Approach for Size Measurement of Particulate (Nano)materials. Materials 12, 2274. https://doi.org/10.3390/ma12142274

Vinogradov, J., Jaafar, M.Z., Jackson, M.D., 2010. Measurement of streaming potential coupling coefficient in sandstones saturated with natural and artificial brines at high salinity. J. Geophys. Res. 115, B12204. https://doi.org/10.1029/2010JB007593

Wagner, M., Scherer, C., Alvarez-Muñoz, D., Brennholt, N., Bourrain, X., Buchinger, S., Fries, E., Grosbois, C., Klasmeier, J., Marti, T., Rodriguez-Mozaz, S., Urbatzka, R., Vethaak, A.D., Winther-Nielsen, M., Reifferscheid, G., 2014. Microplastics in freshwater ecosystems: what we know and what we need to know. Environmental Sciences Europe 26. https://doi.org/10.1186/s12302-014-0012-7

Wagner, S., Reemtsma, T., 2019. Things we know and don't know about nanoplastic in the environment. Nature Nanotechnology 14, 300–301. https://doi.org/10.1038/s41565-019-0424-z

Weiss, T.H., Mills, A.L., Hornberger, G.M., Herman, J.S., 1995. Effect of Bacterial Cell Shape on Transport of Bacteria in Porous Media. Environ. Sci. Technol. 29, 1737–1740. https://doi.org/10.1021/es00007a007

Wu, J., Jiang, R., Lin, W., Ouyang, G., 2019. Effect of salinity and humic acid on the aggregation and toxicity of polystyrene nanoplastics with different functional groups and charges. Environmental Pollution 245, 836–843. https://doi.org/10.1016/j.envpol.2018.11.055

Wu, L., Gao, B., Tian, Y., Muñoz-Carpena, R., Zigler, K.J., 2013. DLVO Interactions of Carbon Nanotubes with Isotropic Planar Surfaces. Langmuir 29, 3976–3988. https://doi.org/10.1021/la3048328

Xu, S., Liao, Q., Saiers, J.E., 2008. Straining of nonspherical colloids in saturated porous media. Environ. Sci. Technol. 42, 771–778. https://doi.org/10.1021/es071328w

Deposition of Environmentally Relevant Nanoplastic Models in Sand during Transport Experiments

Alice Pradel [a*], Hind el Hadri [b], Cloé Desmet[c], Jessica Ponti[c], Stéphanie Reynaud [b], Bruno Grassl [b], Julien Gigault [a*]

[a] *Univ Rennes, CNRS, Géosciences Rennes - UMR 6118, 35000 Rennes, France*
[b] *IPREM, UMR 5254, CNRS-Université de Pau et des Pays de L'Adour, 64000 Pau, France*
[c] *European Commission, Joint Research Centre (JRC), Directorate F - Health, Consumers and Reference Materials, Via E. Fermi 2749, 21027 Ispra, VA, Italy*
**julien.gigault@univ-rennes1.fr*

Highlights

- In order to determine the environmental fate of nanoplastics, models of nanoplastics with environmentally relevant physicochemical properties must be used.
- Nanoplastic models with polymorphic (irregular and asymmetrical) shapes are more likely to be trapped in porous media, than spherical models.
- Shape has a greater impact on the deposition rate than particle size or particle concentration.

Deposition of Environmentally Relevant Nanoplastic Models in Sand during Transport Experiments

Alice Pradel [a*], Hind el Hadri [b], Cloé Desmet[c], Jessica Ponti[c], Stéphanie Reynaud [b], Bruno Grassl [b], Julien Gigault [a*]
[a] *Univ Rennes, CNRS, Géosciences Rennes - UMR 6118, 35000 Rennes, France*
[b] *IPREM, UMR 5254, CNRS-Université de Pau et des Pays de L'Adour, 64000 Pau, France*
[c] *European Commission, Joint Research Centre (JRC), Directorate F - Health, Consumers and Reference Materials, Via E. Fermi 2749, 21027 Ispra, VA, Italy*
**julien.gigault@univ-rennes1.fr*

Declaration of interests

☒ The authors declare that they have no known competing financial interests or personal relationships that could have appeared to influence the work reported in this paper.

☐The authors declare the following financial interests/personal relationships which may be considered as potential competing interests: